electronics

MDPI

Article

$LiNbO_3$ Surface Acoustic Wave Resonators with Large Effective Electromechanical Coupling

Shitian Huang [1], Yao Shuai [1,2,*], Lu Lv [1], Zijie Wei [1], Wei Fan [1], Yuedong Wang [1], Dailei Zhu [1], Xinqiang Pan [1,2], Wenbo Luo [1,2], Chuangui Wu [1,2] and Wanli Zhang [1,2]

[1] School of Integrated Circuit Science and Engineering, University of Electronic Science and Technology of China, Chengdu 610054, China; huangshitian@std.uestc.edu.cn (S.H.); lvlu@std.uestc.edu.cn (L.L.); rivalry970929@163.com (Z.W.); fanwei_fw@163.com (W.F.); thotspur@126.com (Y.W.); zhudailei1127@163.com (D.Z.); panxinqiang@uestc.edu.cn (X.P.); luowb@uestc.edu.cn (W.L.); cgwu@uestc.edu.cn (C.W.); wlzhang@uestc.edu.cn (W.Z.)

[2] State Key Laboratory of Electronic Thin Films and Integrated Devices, University of Electronic Science and Technology of China, Chengdu 610054, China

* Correspondence: yshuai@uestc.edu.cn

Abstract: This paper reports an LNO surface acoustic wave (SAW) resonator based on a shear horizontal mode with high operating frequency over 3 GHz, large electromechanical coupling of 33.54%, Q factor of 380, and a relatively good figure of merit (FOM) of 127. Combing crystal-ion-slicing (CIS) technology with a room temperature bonding method, a 4-inch single crystalline LNO thin film on silicon is prepared successfully. The influence of damaged LNO film on crystalline quality and SAW performance is comprehensively analyzed. After totally removing the damaged layer, the electromechanical coupling and Q factor is significantly improved. The high-performance SAW resonator possesses the potential to meet the requirements of SAW filters for the fifth-generation (5G) communication in terms of high frequency, large bandwidth, and a high-quality factor.

Keywords: 41°YX-cut LNO film; crystal-ion-slicing (CIS); surface acoustic wave (SAW); large electromechanical coupling

check for updates

Citation: Huang, S.; Shuai, Y.; Lv, L.; Wei, Z.; Fan, W.; Wang, Y.; Zhu, D.; Pan, X.; Luo, W.; Wu, C.; et al. $LiNbO_3$ Surface Acoustic Wave Resonators with Large Effective Electromechanical Coupling. *Electronics* **2023**, *12*, 2964. https://doi.org/10.3390/electronics12132964

Received: 23 May 2023
Revised: 27 June 2023
Accepted: 3 July 2023
Published: 5 July 2023

Copyright: © 2023 by the authors. Licensee MDPI, Basel, Switzerland. This article is an open access article distributed under the terms and conditions of the Creative Commons Attribution (CC BY) license (https://creativecommons.org/licenses/by/4.0/).

1. Introduction

As the rapid development of mobile communication, especially in the arrival of the fifth-generation (5G) wireless system, the perfect integration of the Internet of Things, cloud computing, big data, and artificial intelligence represents the general trend [1–4]. Therefore, the devices that make up the 5G wireless system are faced with challenges of miniaturization, low-power consumption, and good compatibility with the integrated circuitry [5–9]. Surface acoustic wave (SAW) devices have become the mainstream implementation of radio frequency (RF) filters in modern mobile transceivers because the SAW devices can fully meet the above requirements in terms of certain components of the wireless system. Different from the 4G communication, SAW filters, which are fabricated by cascading resonators, should have a higher and wider communication frequency band as the explosive increasing of mobile data traffic [10,11]. Because of this, SAW resonators with a high frequency, a large effective electromechanical coupling (k^2), a great temperature stability, and a high-quality factor are necessary [12,13].

Conventionally, SAW devices are fabricated on $LiTaO_3$ and $LiNbO_3$ (LNO) bulk wafers, which do not meet the requirement of high-performance in a 5G wireless system. In order to improve the performance of SAW devices, many studies have been reported. By introducing the solidly mounted resonator (SMR) type into shear horizontal (SH) mode plate wave devices instead of the cavity type, a large electromechanical coupling factor of 54% was achieved [14]. The piezoelectric-on-insulator (POI) layered structure is now utilized to prepare high-performance devices due to its huge advantages. Guide mode

waves, such as the SH mode with high-velocity, can be achieved. At the same time, each layer of the multiple layer processes the unique properties to optimize the SAW devices. For example, the high thermal conductivity Si substrate can enhance the heat dissipation capacity efficiently, and the power durability is improved. The SiO_2 layer plays the role of compensated layer due to its unique feature of positive temperature drift coefficient [15,16]. An incredible high-performance (IHP) SAW device was fabricated successfully with a new multilayered structure (42°YX $LiTaO_3/SiO_2/AlN/Si$). The SiO_2/AlN layer was introduced to highly confine the leaky part of SAW and improves the performance. The IHP SAW showed high Bode-Q values over 1900 at 3.5 GHz, which was over 3 times that of a conventional 42°YX-LTO bulk SAW resonator, and quite a small temperature coefficient of frequency (TCF) was realized [17]. The improved and simplified SAW resonators with a 15°YX LNO film/SiO_2/Si structure was also fabricated, and a high large electromechanical coupling factor of 35.8% was reported [18]. However, the velocity of the SH mode got lower while using Cu interdigital electrodes (IDTs) to minimize the effects of Rayleigh mode and weaken in-band fluctuations for the comprising filters. Nevertheless, the difficulty is preparing special cut angle LNO or LTO films whose crystalline quality is close to the bulk LNO or LTO to meet the requirement of SAW devices. By the conventional depositing methods [19], only films with certain specific orientations can be prepared. Furthermore, the random distribution of grain and the grain boundary in polycrystalline or amorphous films results in the reduction of the SAW performance. The crystal-ion-slicing (CIS) technology has been reported in our previous work [20–22]. High quality single crystalline and arbitrarily cut angle LNO film can be prepared.

In this work, the Al/LNO film/SiO_2/Polysilicon/Si (LNOI) structure is simulated and the influence of the SAW resonator parameters are researched with the Finite element method (FEM). After that, a 4-inch 41°YX-cut LNO single crystalline film is fabricated on high resistivity (HR) silicon, combining CIS technology and the room temperature wafer bonding method. By removing the damaged LNO layer, the quality of LNO film is promoted and very close to the LNO bulk wafer. The LNOI substrate with 41°YX-cut LNO film/SiO_2/Polysilicon/Si structure is used to fabricated SAW resonators. Properties of materials and devices have been studied and analyzed in detail. The resonators with high frequency, a large electromechanical coupling (k^2), and a relatively good figure of merit (FOM) are successfully obtained.

2. Design and Simulation

Figure 1a displays the mock-up view of one-port SAW resonator using the single crystalline 41°YX-cut LNO film on silicon substrate with labelling the key parameters. In order to offer sufficient mechanical reflection, two short circuit grating reflectors (GRs) with N_r metal strips were placed at both sides of interdigital transducers (IDTs), and the gap (g) between the IDT and the GR was set to $\lambda/4$ (λ is the wavelength). The IDTs were composed of N_e pairs of metal fingers with aperture A of 20 λ, pitch P of $\lambda/2$, and width W_e of $\lambda/4$. The parameters in the Table 1 are defined as well. In this paper, we used COMSOL for the FEM simulation. The 2D model with Al/LNO/SiO_2/Polysilicon/Si structure of the SAW resonator was built in COMSOL as shown in Figure 1b. The results were consistent with those in 3D model in Supplementary Information. In order to improve operational efficiency, the perfectly matched layer was introduced. Then, the computational accuracy and efficiency was controlled by adjusting the size of free triangular meshes. Based on multi-physical field coupling (solid mechanics and static electricity), the frequency domain research was taken. Perfect match layer with width of λ was chosen to improve computational efficiency and include the bulk wave radiation loss [23].

The influence of cut angle of LNO on SAW performance was researched by setting the Euler angles in rotational coordinate system, which we could directly call the material parameters corresponding to the tangential direction in the material library. In this paper, the corresponding Euler angles was (0, -theta, 0) while we used (theta)YX cut LNO to simulate the SAW performance. Then, the +X axis was the wave propagation direction.

Based on Al IDT/LNO/SiO_2/Polysilicon/Silicon structure, the influence of different Y-cut angle (0–180°) of LNO film on the electromechanical coupling coefficient and sound velocity was confirmed in Figure 2a. The shear horizontal mode was observed, indicating the SAW resonator could also gain higher k^2 compared with SH_0-SAW resonator [23]. The k^2 was calculated with the following equation:

$$k^2 = \frac{\pi^2}{8} \frac{{f_p}^2 - {f_s}^2}{{f_s}^2} \times 100\% \quad (1)$$

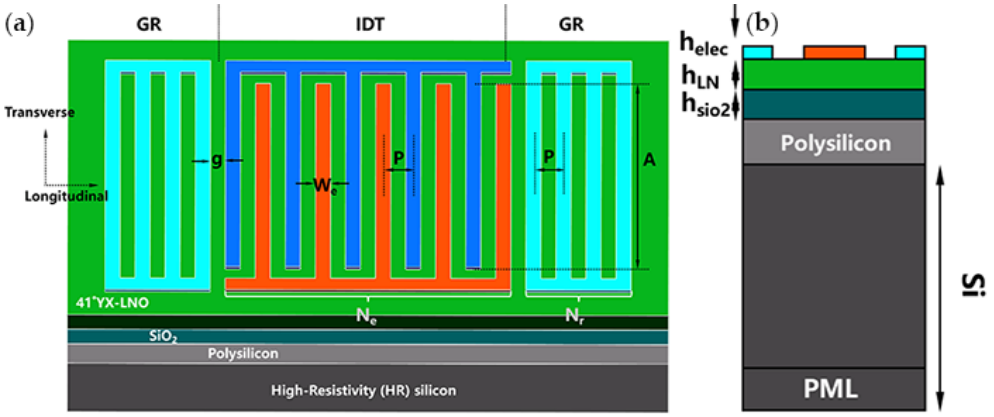


Figure 1. (**a**) the mock-up view of one-port SAW resonator, (**b**) the cross-sectional vies of the LNO SAW resonator based on LNO/SiO_2/Polysilicon/Si for 2D FEM simulation.

Table 1. The parameters in the table are defined in Figure 1a.

Parameters	Value
Pithch (P), Width (We)	$\lambda/2$, $\lambda/4$
# of IDT Pairs (Ne)	70
# of grating (Nr)	20

While the cut angle in the region of 0°–50°, the k^2 and the sound velocity were both high, which meant the SAW resonator was not only suitable for wide band filter, but also could be a good candidate for application on high frequency band. Due to using the Al IDT instead of Cu or Au IDT, the sound velocity of shear horizontal mode wave in LNO film significantly improved, and the maximum value reached 4000 m/s. The admittance ratio (AR = Resonance admittance/Anti-resonance admittance) of the SH-SAW resonator was also quite high while the cut angle in the region of 0°–60°, indicating that good performance with high Q factor could be achieved, as shown in Figure 2b. Considering the commercial availability of LNO wafer, the 41°YX-LNO was chosen to fabricate the SAW resonator in our paper. Figure 2c shows that the k^2 decreased rapidly by increasing the LNO film thickness. On the contrary, the sound velocity increased as the increasing 41°YX-LNO film thickness varied from 0.083 λ to 0.41 λ and then slightly decreased while using the Al IDT. As Figure 2d shows, the spurious mode could be kept apart from the shear horizontal mode and even eliminated while the LNO thickness varied from 0.83 λ to 0.33 λ. The Rayleigh mode was almost not observed near the position of the shear horizontal mode.

Figure 3a demonstrates the influence of Al IDT thickness on k^2 and sound velocity. The value of k^2 and sound velocity both rapidly decreased as the Al IDT thickness increased from 0.06 λ to 0.2 λ. In order to achieve higher k^2 and sound velocity, the preferred Al IDT thickness should be chosen from 0.06 λ to 0.12 λ. Figure 3b proves that the spurious mode can be controlled far from the passband of filters by regulating the Al IDT thickness. While increasing the SiO_2 thickness from 0.33 to 1.67 h_{LNO}, k^2 and sound velocity have little change, and the Rayleigh mode also seems to be weak in Figure 3c. Figure 3d shows

that there was no obvious influence on performance of resonator while changing thickness of the polysilicon, which has been reported as the role of trap-rich layer [24] that will limit high frequency signal propagation in the substrate. Therefore, according to the above FEM simulation results, the thickness of each layer of Al IDT/LNO/SiO_2/Polysilicon/Silicon structure was set up as 140 nm, 280 nm, 280 nm, and 500 nm.

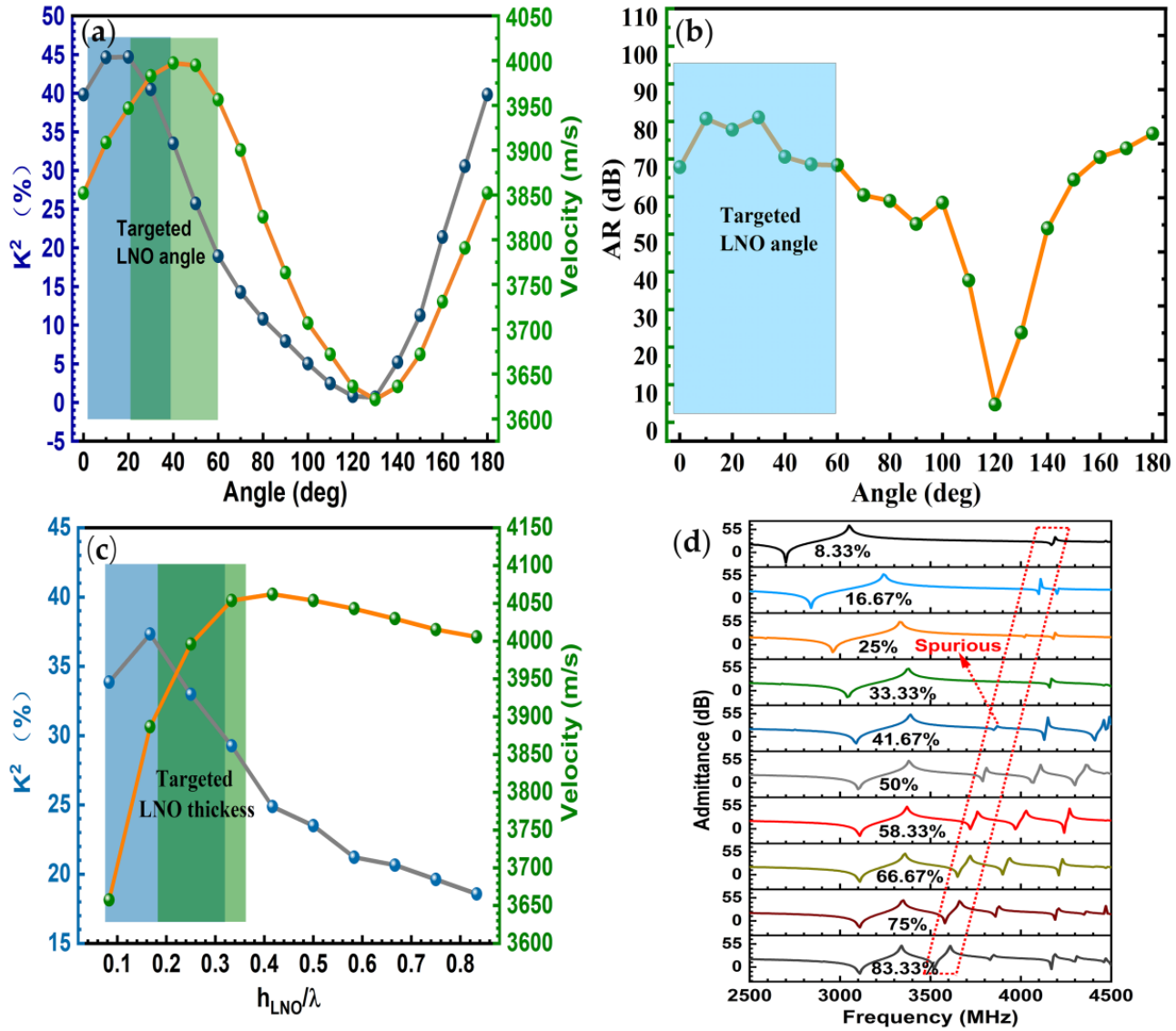


Figure 2. (**a**) The influence of different Y-cut angle (0°–180°) of LNO film on the electromechanical coupling coefficient and sound velocity, (**b**) The admittance ration (AR) of the SH-SAW resonator with the cut angle in the region of 0°–180°, (**c**) the influence of different thickness of LNO film on the electromechanical coupling coefficient and sound velocity, (**d**) the influence of thickness on improving the distribution of the spurious mode.

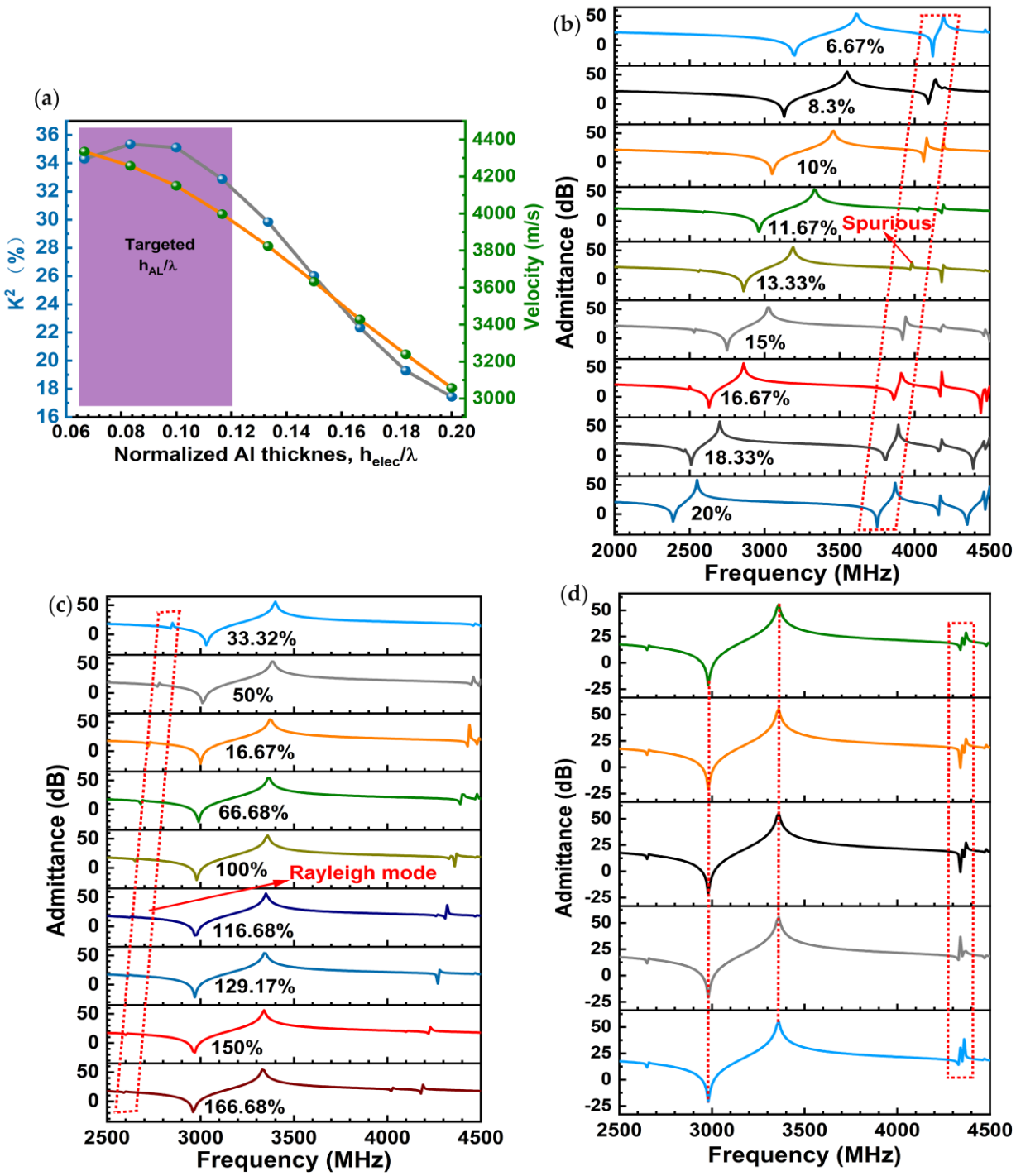


Figure 3. (**a**) The influence of Al IDT thickness on the electromechanical coupling coefficient and sound velocity, (**b**) the improvement of the distribution of the spurious mode by regulating the Al IDT thickness, the influence of (**c**) SiO_2 thickness, and (**d**) Polysilicon thickness on resonator performance by FEM simulation.

3. Experiment

A 4-inch single crystalline 41°YX-cut LNO film was transferred onto high resistivity silicon (100) substrate by CIS technology. The fabrication process is shown in Figure 4a–e. First, as shown in Figure 4a, 41°YX-cut LNO wafer was implanted by He^+ ions. The implantation energy was 100 keV, and the implantation dose was 2×10^{16} cm^{-2}. Then, 500 nm thick polysilicon was deposited on silicon substrate by Low Pressure Chemical

Vapor Deposition (LPCVD) and then 280 nm thick SiO_2 film was grown with chemical vapor deposition (CVD). After that, the surface was polished by Chemical Mechanical Polishing (CMP) in order to reduce the surface roughness to satisfy the requirement of room temperature (RMS < 0.5 nm). [25] Before bonding as shown in Figure 4b, the implanted LNO wafer and the Si (100) substrate with depositing SiO_2 and polysilicon film were rinsed using ultrasonic and megasonic DI water to remove the residual particles. Then, the bonding surfaces are activated by N_2 plasma for 45 s. After surface activation, the ultrasonic and megasonic DI water rinsing was applied to the bonding surfaces again. Following, the implanted LNO wafer and the Si substrate were aligned, attached, and bonded at room temperature. In order to keep timeliness of plasma activation, the whole process of bonding was completed in a relatively short period of time. To ensure the LNO film transferring onto the substrate, the bonding strength was enhanced by annealing at 120 °C for 20 h. After annealing at 180 °C for 10 h, the single crystalline 41°YX-cut LNO film was exfoliated from the implanted LNO wafer and transferred onto the Si substrate, as shown in Figure 4c. After transferring the LNO film, the wafer with LNO film/SiO_2/Polysilicon/Si structure annealing at 400 °C for 10 h under oxygen atmosphere. Finally, the surface is smooth and the damaged layer was removed by CMP at the same time as shown in Figure 4d,e. In order to fabricate one-port SAW resonator, conventional lithography and lift-off process were necessary based on the fabricated wafers with 41°YX-cut LNO/SiO_2/Polysilicon/Si structure.

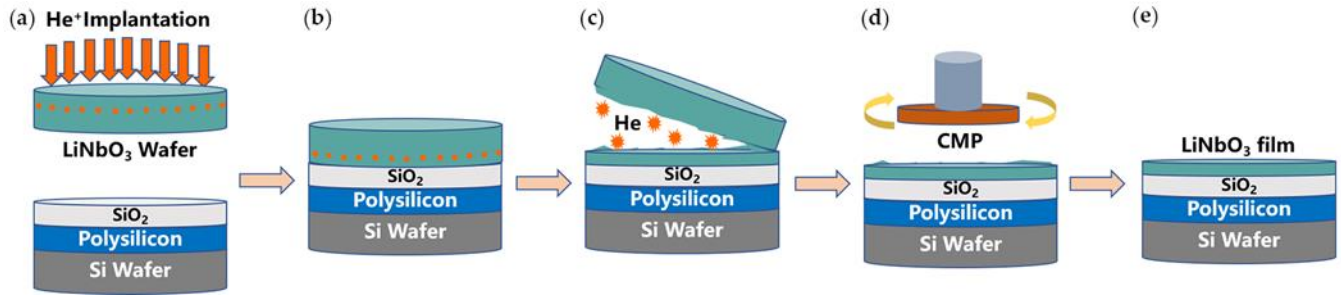


Figure 4. (**a**–**e**) The fabrication process of LNO single crystalline film, (**a**) 41°YX-cut LNO wafer implanted by He^+ ions and SiO_2 film deposited following the process of depositing polysilicon film on 4-inch high resistivity silicon wafer, (**b**) room temperature bonding of the implanted LNO wafer and the Si substrate with SiO_2/polysilicon/Si structure, (**c**) the implanted LN exfoliated along the He^+-induced damage region after annealing process, (**d**) the smooth surface and the damaged layer removing by Chemical Mechanical Polishing (CMP).

The micro morphology was measured with atomic force microscopy (AFM, SPI-3800N) and X-ray diffraction (XRD, Agilent Xcalibur E), respectively. The cross-sectional microstructure of the LNO film and the lattice arrangement are characterized by cross-sectional transmission electron microscopy (XTEM, Talos F200x, FEI) and the TEM sample was prepared with the focused ion beam (ZEISS Crossbeam 540) process. The thickness was measured with reflection interferometer (Filmetric 50). The structure of Al IDTs was measured with Laser confocal (Sneox-3D). The SAW resonator was tested with vector Analyzer (Keysight, E5071C) and 150-μm-pitch GS probe (Cascade Microtech). With the SLOT calibration method, the vector network analyzer was calibrated using four parts on probe card: short circuit, load, open circuit, and straight through. After calibration, the SAW resonators were done chip probing.

4. Results and Discussion

In order to realize the transferring of LNO film, He^+ is implanted into the LNO wafer, and the damaged layer with He^+ is introduced under the LNO wafer [26]. After annealing, the blistering phenomenon is observed, and He bubbles grow and expand to the whole wafer. Finally, the He bubbles break and the LNO film is transferred onto the Si substrate.

Therefore, the rough surface and the damaged layer near the LNO film surface exist. CMP technology is the best method to remove the damaged layer and smooth at the same time in wafer scale. According to the results of FEM simulation, the LNO film thickness affects not only the k^2, but also the sound velocity. Therefore, detailed characterization of the damaged layer of LNO film should be performed. A high-resolution XTEM image of pristine LNO film is shown in Figure 5a,b. A damaged layer with maximum thickness of around 100 nm is formed and clearly different from the LNO film. Twins appearing in local areas and the result of selected area electron diffraction image in the inset of Figure 5b both indicate that the LNO film with a width damaged layer has a low single crystalline quality. Figure 5c,d shows that the damaged layer has been partially removed and its thickness is about 60 nm. Locally penetrating microcracks are also observed, indicating the damaged LNO film is very fragile and holds very low mechanical strength. The cavity also appears and the selected area electron diffraction image in the inset of Figure 5d proves that the crystal quality has not been improved effectively yet. By adjusting and optimizing the CMP process, the damaged layer can be completely removed, and a 280 nm thick LNO film remains in Figure 5e. A well-oriented single crystalline LNO film is observed without obvious defects, and the selected area electron diffraction image in the inset of Figure 5f confirms that the LNO film holds high single crystalline quality. In order to verify the improvement of crystalline quality, XRD rocking curves of the single crystalline LNO films are shown in Figure 6a–d. The full width at half maximum (FWHM) of the rocking curve of LNO bulk is 59.004 arcsec, indicating the LNO wafer owns high single crystalline quality in Figure 6a. As shown in Figure 6b, the FWHM of the rocking curve of the initial LNO film without CMP is 124.992 arcsec, which is more than twice that of the LNO bulk and shows that the quality of LNO films considerably differ from the bulk due to the damaged LNO layer in Figure 5a.

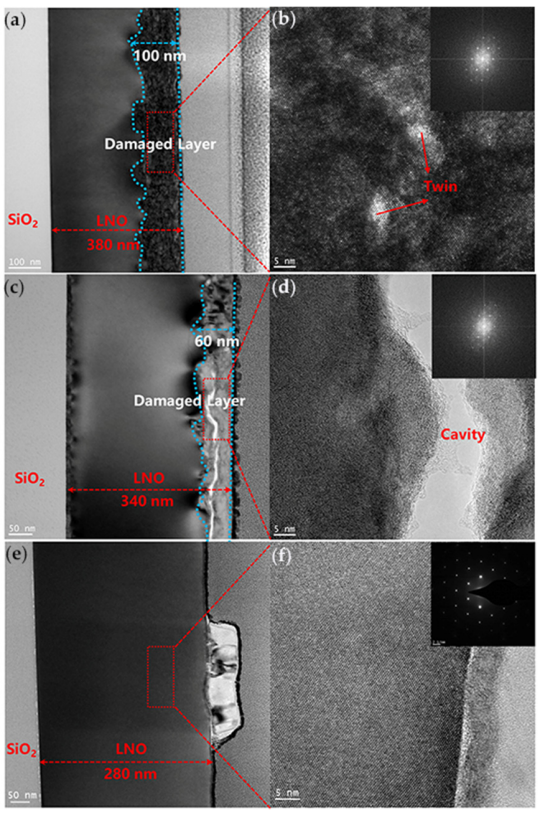


Figure 5. (**a**) Damaged layer with maximum thickness of around 100 nm after transferring LNO film, (**b**) image and, (**c**) the 60 nm thickness damaged layer after CMP, (**d**) the cavity and microcracks measured by High-resolution XTEM and selected area electron diffraction image of the damaged layer in the inset, (**e**) the damaged layer completely removed and 280 nm thick LNO film, (**f**) Well oriented single crystalline LNO film by High-resolution XTEM and selected area electron diffraction image in the inset.

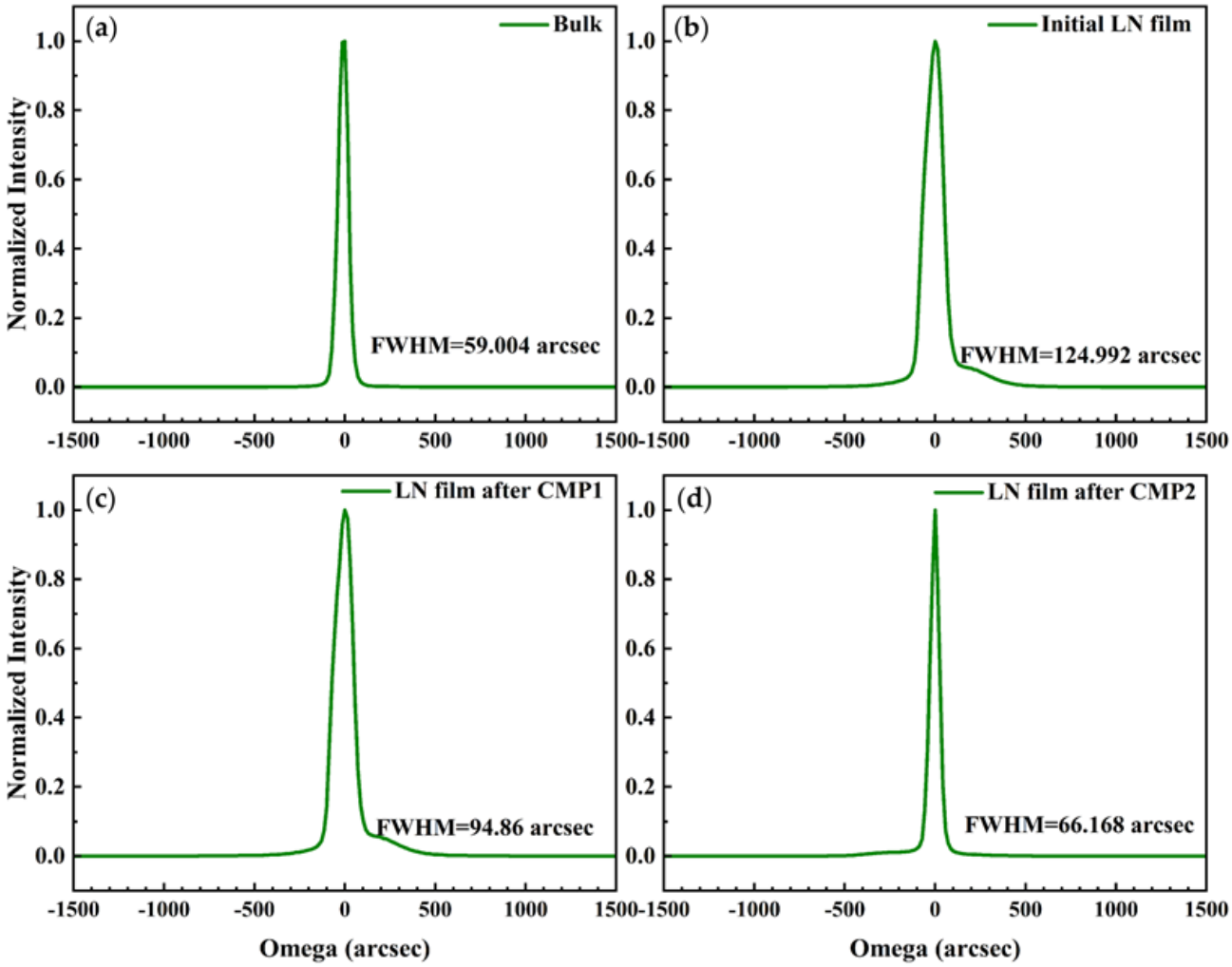


Figure 6. XRD rocking curves of the LNO bulk wafer and single crystalline LNO films, (**a**), the LNO bulk wafer, (**b**) the initial LNO film without CMP, (**c**) the LNO film with the 60 nm thick damaged layer, (**d**) the LNO film with completely removing the damaged layer.

Figure 6c shows that the FWHM of 94.86 arcsec slightly reduced after CMP1 while the thickness of the damaged LNO layer still reaches 60 nm. As shown in Figure 6d, the FWHM is reduced to 66.168 arcsec and the LNO film holds high quality, which is very close to the LNO bulk after CMP2 process while completely removing the damaged layer.

As shown in Figure 7a, the surface roughness (RMS) of the initial LNO film peeling off from the bulk LNO is 11.16 nm, which is caused by the formation of microcrack layer during annealing. While the damaged layer is partially removed, the RMS rapidly decreases and reaches at 1.46 nm, as shown in Figure 7b. However, such RMS at this level is still too large for fabricating the high-performance SAW devices, and the RMS below 0.5 nm is preferred. Further, the roughness is further reduced to 0.28 nm, which is satisfactory to serve as the SAW ready surface [26] after, as shown in Figure 7c. Figure 7d shows the image of the 4 inch 41°YX-cut LNO film on HR silicon (100) after removing the whole damaged LNO layer, and no visible defects were induced. The thickness of LNO film is characterized by an automated film thickness mapping system, and the thickness uniform with 47 distributed points on the surface is measured as shown in Figure 7e.

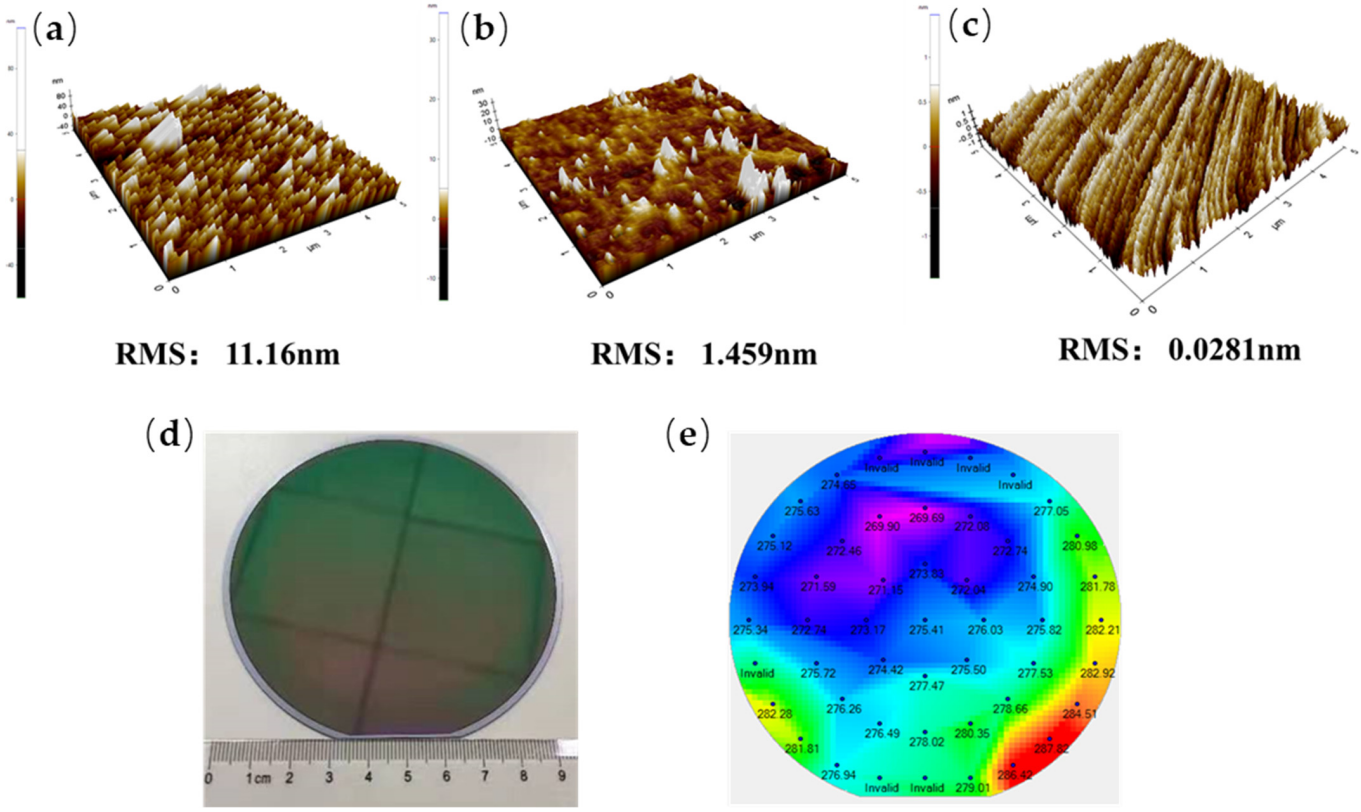


Figure 7. The surface roughness (RMS) of (**a**) the initial LNO film peeling off from the bulk LNO, (**b**) the LNO film with damaged layer partially removed, (**c**) the LNO film with damaged layer completely removed, (**d**) the image of the 4-inch 41°YX-cut LNO film on HR silicon (100) after removing the whole damaged LNO layer, (**e**) the thickness mapping of LNO film.

The average thickness is 274 nm, and the uniformly is ±1.5% according to following equation:

$$\text{Uniform} = \frac{T_{max} - T_{min}}{2T_{mean}} \times 100\% \quad (2)$$

where T_{max}, T_{min}, and T_{mean} are the maximum thickness, minimum thickness, and average thickness, respectively. Under the guidance of FEM simulation, one-part SAW resonators based on Al IDT/41°YX-cut LNO/SiO_2/Polysilicon/HR-Silicon are fabricated. Figure 8a showed the typical image of the LNO SAW resonator. Morphological characteristics of local electrode areas is performed in Figure 8b. The optical microscope images exhibit the complete topology of the resonator with IDTs and reflectors. The uniform device confirms the high-quality fabrication. The fabricated LNO SAW resonators are tested in ambient dry air with a Keysight E5071C ENA network analyzer and GSG probes. In order to research the influence of the damaged LNO layer on the performance of the SAW resonator, an LNOI wafer with 340 nm thick LNO film, which owns a 60 nm damaged layer, is also used for fabricating the SAW resonator while keeping other parameters unchanged. Figure 9a depicts the measured admittance of SH-SAW resonators. The resonator exhibits a center frequency of 3235 MHz (λ = 1.2 μm) with quite low k^2, admittance ratio (AR), and Q_{max} factor of 2.07%, 17.768 dB, and 99. The Q factor is calculated as the following equation:

$$Q(f) = \frac{2\pi f \times \tau(f) \times |\, S11 \,|}{1 - |\, S11 \,|^2} \quad (3)$$

where τ is the group delay of the measured S11. The Q factor is calculated first, and then, the max value (Q_{max}) is achieved at anti-resonance. While using an LNOI wafer

with 280 nm thick LNO film, which owns no damaged layer in Figure 5e, the resonator exhibits a center frequency of 3164 MHz (λ = 1.2 µm) with quite a high k^2, AR, and Q_{max} factor of 33.54%, 59.017 dB, and 380, resulting in a good FOM (= $k^2 \times Q_{max}$) of 127, as shown in Figure 9b. The above results of SAW resonators that center resonant frequency slightly increased due to the bigger velocity of the hear horizontal mode wave increasing the thickness of the LNO film and is consistent with the FEM simulation results in Figure 2d. Because the lattice damage of the LNO crystalline, the piezoelectric performance of the LNO film is deteriorated, which indicates that the k^2 significantly reduces and the energy loss exacerbates it. The electrode loss increases due to the big RMS while the damaged layer remains. To clearly understand the impact of damaged layers on the SAW resonator performance, the modified Butterworth–Van Dyke (MBVD) equivalent circuit model is employed to characterize the resonance behavior. In the model, the series motional branch, consisting of the motional resistance (R_m), capacitance (C_m), and inductance (L_m), describes the mechanical resonance. C_0, R_0, and R_s generally represent the static capacitance between the IDT fingers, parasitic resistance of materials, and resistance from electrodes and contact pads, respectively [27]. Figure 9a,b also showed the fitting admittance curves of the MBVD model. Meanwhile, the equivalent circuit parameters, which are obtained by fitting the measured data with the MBVD model, are shown in Table 2. The fitted MBVD equivalent circuit parameters. By comparison, it is obvious that all the parameters have changed and the value of C_m, L_m, and R_m show changes in the order of magnitude after the damaged layer was totally removed. While the C_m and L_m make great changes after totally removing the damaged LNO layer, the k^2 significantly increases from 2.07% to 33.54%. The values of R_s and R_0 affect the admittance of resonance and antiresonance points, respectively. Figure 9d displays the significant difference in the SAW performance with the damaged layer and removing that after the CMP process.

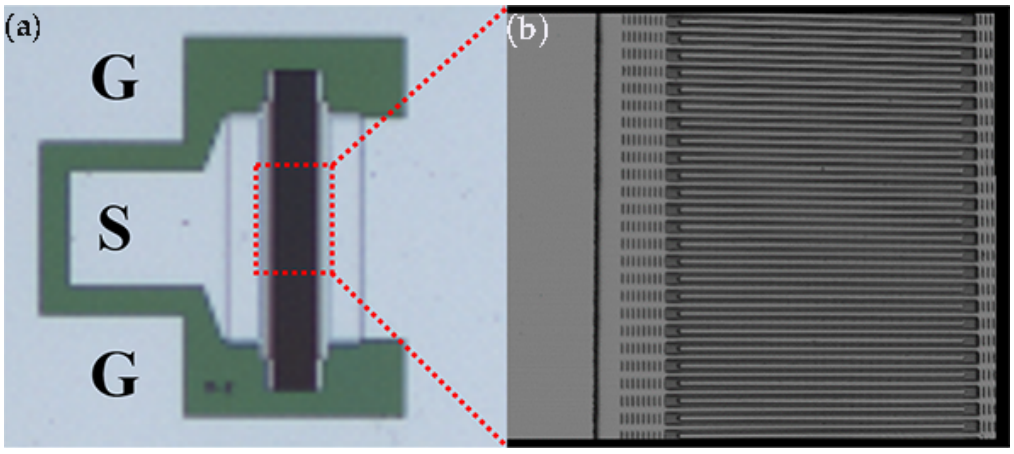


Figure 8. (**a**) The typical image of the LNO SAW resonator, (**b**) morphological characteristic of local electrode areas.

Table 2. The fitted MBVD equivalent circuit parameters.

Damage Layer	C_0 (pF)	C_m (pF)	L_m (nH)	R_m (Ω)	R_0 (Ω)	R_s (Ω)
With	1.37984	0.023222	105	11.7986	5.2567	0.6056
Without	3.19501	0.860134	3.32	−0.2522	0.4640	1.3792

Figure 10a displays the simulated admittance curves of LNO SH-SAW resonators with different wavelengths varying from 1 µm to 1.3 µm. The values of AR under different wavelengths approach 75 dB and indicate that the SAW resonator holds good potentiality for high performance. Figure 10b shows the measured admittance curves and the values of AR approach 60 dB. The measured resonant frequencies under different wavelengths are consistent with that of the simulation. As shown in Figure 10c, the influence of the h_{LN}/λ

is proved by experiments, which are consistent with the results that the k^2 gets further enhanced as h_{LN}/λ approaches 0.21 in Figure 2d with an FEM simulation. Figure 10d shows that the h_{LN}/λ also makes no difference on the Q_{max} factor.

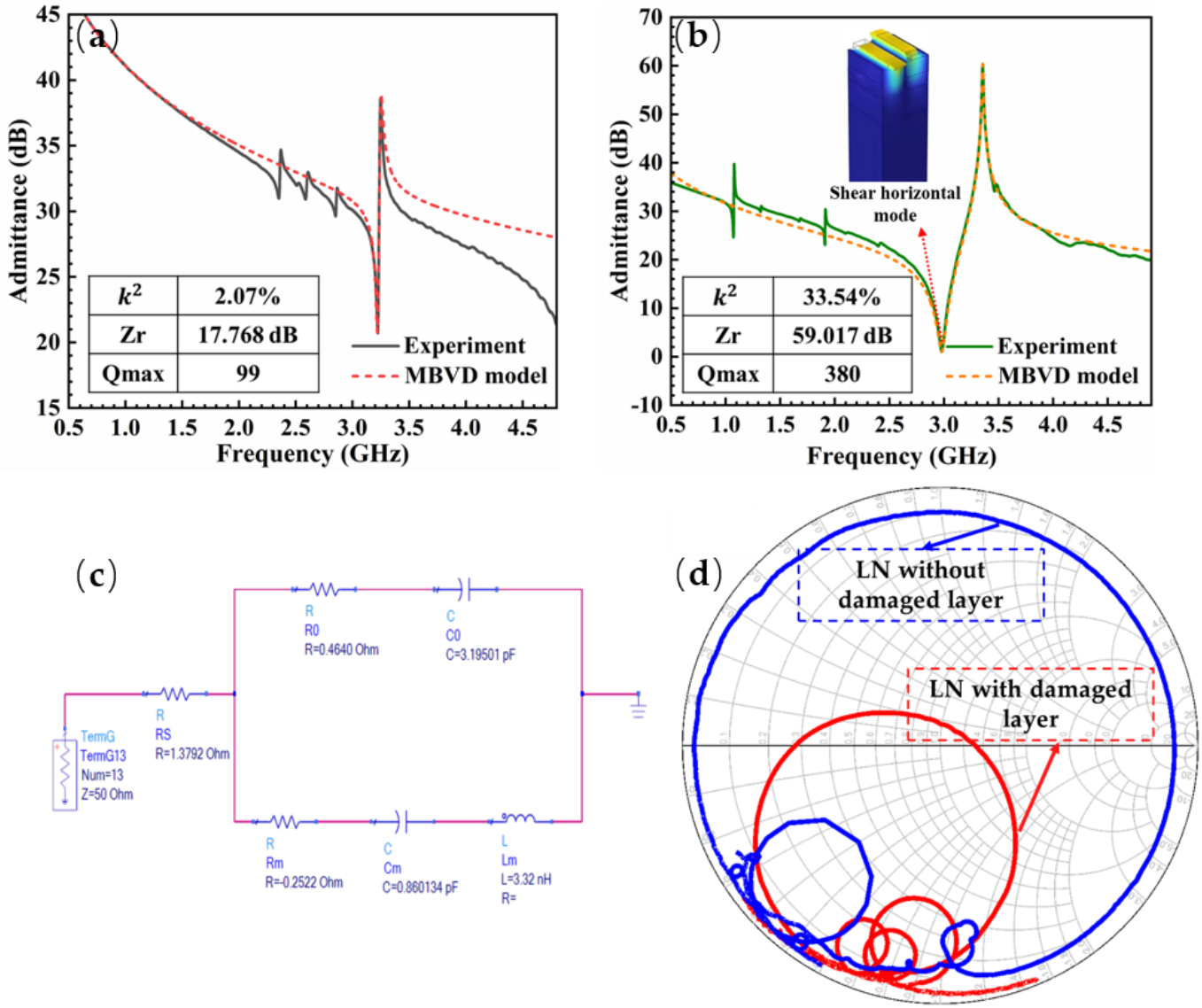


Figure 9. The measured admittance and fitting curves of (**a**) LNO film with 60 nm thick damaged layer and (**b**) no damaged layer, (**c**) the MBVD model, (**d**) Smith chart of SAW resonator with LNO damaged layer and without damaged layer.

Figure 11a,b show the measured admittance curves and Smith chart of the two SH-SAW resonators in different LNOI substrates with different thicknesses of SiO_2 (Sample1 and Sample 2). As an optimizing thickness ratio of SiO_2 and LNO (h_{SiO2}/h_{LNO} = 1), we find that the k^2 is improved by 22.7%, but the Rayleigh mode appears to thicken the SiO_2, which is consistent with the FEM results in Figure 3c. Finally, Table 3 provides a comparison between our work based on the LNOI substrate at an ultra-high-frequency band. Although resonators in [14] exhibit the biggest k^2, the complex fabrication process of the ML reflectors is very challenging and costly. In this work, our SAW resonator performs with large effective electromechanical coupling (33.54%) at a higher frequency (about 3GHz), indicating that the resonator can work at an ultra-high-frequency band belonging to the fifth-generation wireless systems. At the same time, the highest Q_{max} factor makes the highest FOM value, which can further reduce the loss of the filter.

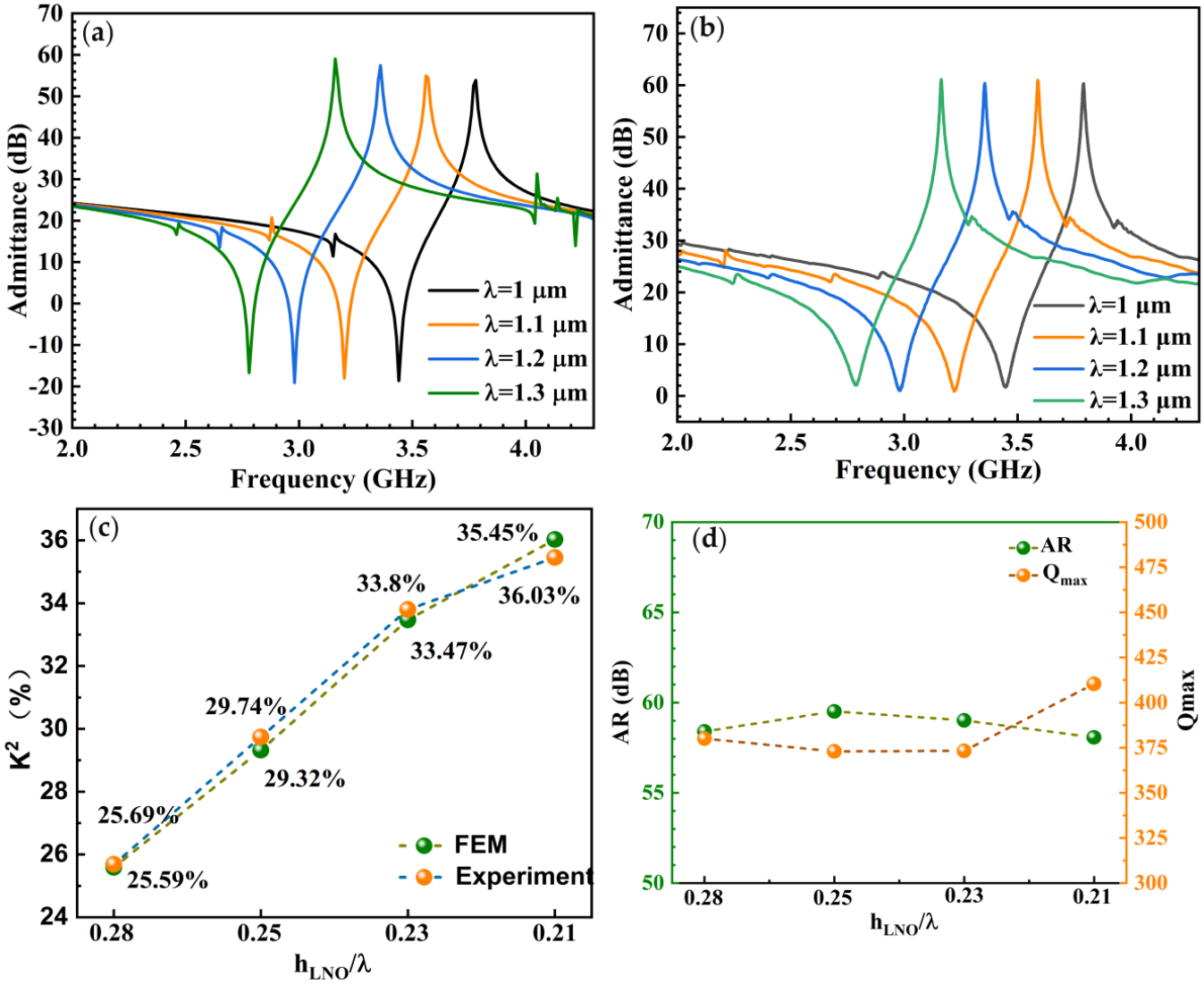


Figure 10. (**a**) The FEM method simulated results and (**b**) the measured of LNO SH-SAW resonators with different wavelengths, the influence of the h_{LN}/λ on (**c**) the k^2 and (**d**) the Q factor.

Table 3. The comparison of LNO resonators.

Reference	Type	F_s (MHz)	k^2	Q_{max}	FOM
[23]	LNO SH0-SAW	713	31.7%	125	40
[14]	LNO/ML SAW	570	54%	--	--
[18]	LNOI SAW	832	36.5%	251	91.615
This work	LNOI SAW	2974	33.54%	380	129

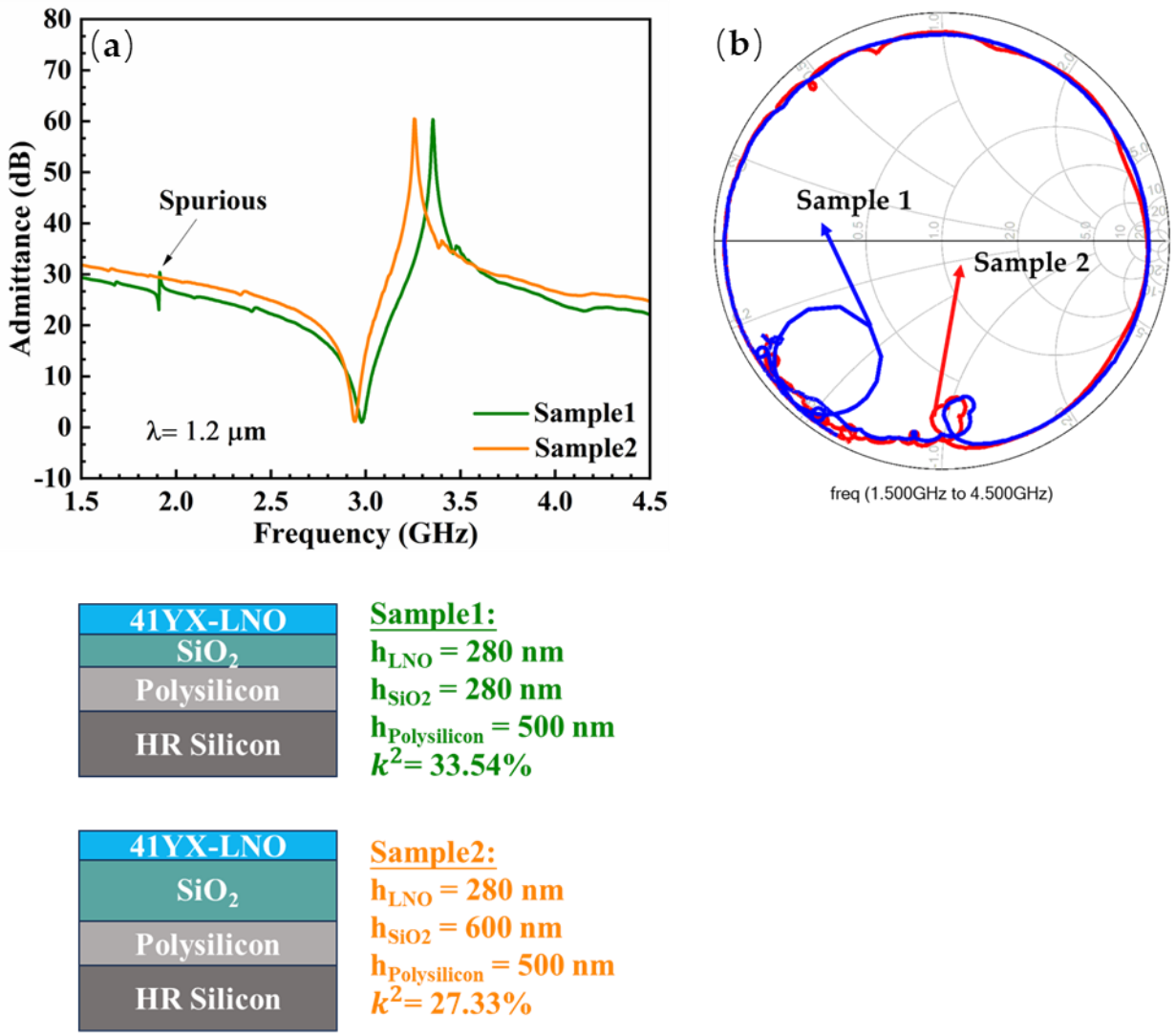


Figure 11. (**a**) The measure admittance curves and (**b**) Smith Chart of Sample1 and Sample2, (**c**) the comparison of the two SH-SAW resonators with different thickness of SiO_2.

5. Conclusions

In this paper, the design of SH-SAW LNO resonators based on a 41°YX-cut LNO film/SiO_2/Polysilicon/Si functional substrate is proposed. With an FEM simulation, the optimum design window was determined and then confirmed by the experiments. The fabricated LNO resonators operated on 3–4 GHz show k^2 of 33.54% and Q of 380, which is suitable for wideband band-pass or band-stop RF front–end filter applications, especially in an N78 frequency band. With the CMP process, the SAW performance is improved significantly, especially in k^2. By optimizing the h_{LNO}/h_{SiO2}, we should make a balance with large k^2 and weak spurious far away the main resonant mode.

Supplementary Materials: The following supporting information can be downloaded at: https://www.mdpi.com/article/10.3390/electronics12132964/s1.

Author Contributions: S.H. contributed the idea, analysis, measurement, simulation and Paper writing; Y.S. contributed the analysis and idea; L.L., Z.W., W.F., Y.W. and D.Z. assisted in the fabrication; X.P., W.L., C.W. and W.Z. contributed the idea and assisted in the work development. All authors have read and agreed to the published version of the manuscript.

Funding: This work was funded by the National Key Research and Development Program of China, grant number 2017YFB0406402. This work was funded by the Nation Natural Foundation of China, grant number 51772044.

Data Availability Statement: The data are not publicly available due to a non-disclosure agreement.

Conflicts of Interest: No conflict of interest relevant to this report.

References

1. Lu, R.; Yang, Y.; Link, S.; Gong, S. Enabling Higher Order Lamb Wave Acoustic Devices with Complementarily Oriented Piezoelectric Thin Films. *J. Microelectromech. Syst.* **2020**, *29*, 1332–1346. [CrossRef]
2. Plessky, V.; Yandrapalli, S.; Turner, P.J.; Villanueva, L.G.; Koskela, J. 5 GHz laterally-excited bulk-wave resonators (XBARs) based on thin platelets of lithium niobate. *Electron. Lett.* **2019**, *55*, 98–100. [CrossRef]
3. Ruby, R. A Snapshot in Time: The Future in Filters for Cell Phones. *Microw. Mag. IEEE* **2015**, *16*, 46–59. [CrossRef]
4. Wang, L.; Chen, S.; Zhang, J.; Xiao, D.; Han, K.; Ning, X.; Liu, J.; Chen, Z.; Zhou, J. Enhanced performance of 17.7 GHz SAW devices based on AlN/diamond/Si layered structure with embedded nanotransducer. *Appl. Phys. Lett.* **2017**, *111*, 253502. [CrossRef]
5. Fu, S.; Wang, W.; Qian, L.; Li, Q.; Lu, Z.; Shen, J.; Song, C.; Zeng, F.; Pan, F. High Frequency Surface Acoustic Wave Devices Based on ZnO/SiC Layered Structure. *IEEE Electron Device Lett.* **2018**, *40*, 103–106. [CrossRef]
6. Lin, C.M.; Chen, Y.Y.; Pisano, A.P.; Senesky, D.G.; Felmetsger, V.V. AlN/3C-SiC composite plate enabling high-frequency and high-Q micromechanical resonators. *Adv. Mater.* **2012**, *24*, 2722–2727. [CrossRef]
7. Luo, J.T.; Zeng, R.; Pan, R.; Li, R.F.; Niu, R.B.; Jia, R.; Liu, R. Filtering performance improvement in V-doped ZnO/diamond surface acoustic wave filters. *Appl. Surf. Sci.* **2010**, *256*, 3081–3085. [CrossRef]
8. Su, R.; Fu, S.; Lu, Z.; Shen, J.; Xu, H.; Mao, H.; Xu, Z.; Song, C.; Zeng, F.; Wang, W. Near 30% fractional bandwidth surface acoustic wave filters with novel electrode configuration. *Prog. Nat. Sci. Mater. Int.* **2021**, *31*, 852–857. [CrossRef]
9. Wang, W.; Zhang, X.; Shui, Y.; Zhang, D.; Han, T. Study on the bulk wave radiation of finite-length SAW devices using FEM/BEM. *Prog. Nat. Sci.* **2005**, *15*, 402–406.
10. Gao, A.; Liu, K.; Liang, J.; Wu, T. AIN MEMS filters with extremely high bandwidth widening capability. *Microsyst. Nanoeng.* **2020**, *6*, 74. [CrossRef]
11. Ji, X.J.; Xiao, Q.; Chen, J.; Wang, H.L.; Omori, T.; Changjun, A. Suppression of Rayleigh wave spurious signal in ultra-wideband surface acoustic wave devices employing $0.67Pb(Mg_{1/3}Nb_{2/3})O_3$-$0.33PbTiO_3$ single crystals. *AIP Adv.* **2017**, *7*, 055013. [CrossRef]
12. Ruppel, C. Acoustic Wave Filter Technology—A Review. *IEEE Trans. Ultrason. Ferroelectr. Freq. Control* **2017**, *64*, 1390–1400. [CrossRef]
13. Shen, J.; Fu, S.; Su, R.; Xu, H.; Pan, F. High-Performance Surface Acoustic Wave Devices Using LiNbO/SiO/SiC Multilayered Substrates. *IEEE Trans. Microw. Theory Tech.* **2021**, *69*, 3693–3705. [CrossRef]
14. Kadota, M.; Tanaka, S. Simulation of solidly mounted plate wave resonator with wide bandwidth using 0-th shear horizontal mode in $LiNbO_3$ plate. *Jpn. J. Appl. Phys.* **2015**, *54*, 07HD09.01–07HD09.04. [CrossRef]
15. Lu, Z.; Fu, S.; Chen, Z.; Shen, J.; Su, R.; Wang, R.; Song, C.; Zeng, F.; Wang, W.; Pan, F. High-frequency and high-temperature stable surface acoustic wave devices on ZnO/SiO_2/SiC structure. *J. Phys. D Appl. Phys.* **2020**, *53*, 305102. [CrossRef]
16. Liu, Y.; Liu, J.; Wang, Y.; Lam, C.S. A Novel Structure to Suppress Transverse Modes in Radio Frequency TC-SAW Resonators and Filters. *IEEE Microw. Wirel. Compon. Lett.* **2019**, *29*, 249–251. [CrossRef]
17. Takai, T.; Iwamoto, H.; Takamine, Y.; Nakao, T.; Koshino, M.I.H.P. SAW technology and its application to micro acoustic components. In Proceedings of the 2017 IEEE International Ultrasonics Symposium (IUS), Washington, DC, USA, 6–9 September 2017.
18. Hsu, T.H.; Tseng, K.J.; Li, M.H. Large Coupling Acoustic Wave Resonators Based on $LiNbO_3/SiO_2$/Si Functional Substrate. *IEEE Electron Device Lett.* **2020**, *41*, 1825–1828. [CrossRef]
19. Bousquet, M.; Perreau, P.; Maeder-Pachurka, C.; Joulie, A.; Reinhardt, A. Lithium niobate film bulk acoustic wave resonator for sub-6 GHz filters. In Proceedings of the 2020 IEEE International Ultrasonics Symposium (IUS), Las Vegas, NV, USA, 7–11 September 2020.
20. Bai, X.; Shuai, Y.; Lv, L.; Huang, S.; Zhang, W. Mo/Ti multilayer Bragg reflector for $LiNbO_3$ film bulk acoustic wave resonators. *J. Appl. Phys.* **2020**, *128*, 094503. [CrossRef]
21. Huang, S.; Luo, W.; Bai, X.; Lv, L.; Zhang, W. A Solidly Mounted Resonator Fabricated by $LiNbO_3$ Single Crystalline Film on Flexible Polyimide Substrate. *IEEE Trans. Ultrason. Ferroelectr. Freq. Control* **2021**, *68*, 2585–2589. [CrossRef] [PubMed]
22. Lv, L.; Shuai, Y.; Huang, S.T.; Zhu, D.L.; Wang, Y.D.; Luo, W.B.; Pan, X.Q.; Wu, C.G.; Zhang, W.L. Area Dependence of Effective Electromechanical Coupling Coefficient Induced by On-Chip Inductance in LiNbO3-Based BAW Resonators. *Electronics* **2022**, *11*, 4032. [CrossRef]
23. Wang, R.; Bhave, S.A.; Zhgoon, S.; Bhattacharjee, K. Multi-frequency LiNbo3 Lamb wave resonators with < 3Ω impedance. In Proceedings of the 2016 IEEE 29th International Conference on Micro Electro Mechanical Systems (MEMS), Shanghai, China, 24–28 January 2016.
24. Butaud, E.; Laroche, T.; Barec, V.; Clairet, A.; Didier, C. A Single Smart Cut POI Substrate Design for UHF, L and S Band Filters. In Proceedings of the 2020 50th European Microwave Conference (EuMC), Utrecht, The Netherlands, 12–14 January 2021.

25. Huang, S.; Luo, W.; Pan, X.; Zhao, J.; Qiao, S.; Shuai, Y.; Zhang, K.; Bai, X.; Niu, G.; Wu, C. Resistive Switching Effects of Crystal-Ion-Slicing Fabricated $LiNbO_3$ Single Crystalline Thin Film on Flexible Polyimide Substrate (Adv. Electron. Mater. 9/2021). *Adv. Electron. Mater.* **2021**, *7*, 2170036. [CrossRef]
26. Yan, Y.; Huang, K.; Zhou, H.; Zhao, X.; Ou, X. Wafer-scale fabrication of 42° rotated Y-cut $LiTaO_3$-On-Insulator (LTOI) substrate for SAW resonator. *ACS Appl. Electron. Mater.* **2019**, *1*, 1660–1666. [CrossRef]
27. Huang, F.; Zhang, W.X.; Li, L.; Sun, Z.F.; Yang, Y.T.; Chen, R.C.; Peng, B.; Zhang, W.L. MEMS Surface Acoustic Wave Resonator Based on AlN/Si/Fe-Co-Si-B Structure for Magnetic Field Sensing. *IEEE Sens. J.* **2022**, *22*, 22510–22518. [CrossRef]

Disclaimer/Publisher's Note: The statements, opinions and data contained in all publications are solely those of the individual author(s) and contributor(s) and not of MDPI and/or the editor(s). MDPI and/or the editor(s) disclaim responsibility for any injury to people or property resulting from any ideas, methods, instructions or products referred to in the content.